# AIAA 97-0566
# Investigation of Differences Between Measured and Predicted Pressures in AEDC/VKF Hypersonic Tunnel B

James R. Maus
Sverdrup Technology, Inc., AEDC Group
Arnold Engineering Development Center
Arnold Air Force Base, Tennessee 37389



**35th Aerospace Sciences Meeting and Exhibit**
January 6-10, 1997 / Reno, NV

# Investigation of Differences Between Measured and Predicted Pressures in AEDC/VKF Hypersonic Tunnel B*

*James R. Maus***
*Sverdrup Technology, Inc., AEDC Group*
*Arnold Engineering Development Center*
*Arnold Air Force Base, TN 37389-6001*

## Abstract

A study has been carried out to assess the effect of flow nonuniformities in AEDC Tunnel B on surface pressures of slender bodies. The approach taken was to use flow profiles measured in a recent calibration program as inflow boundary conditions for a CFD solution to compare with the idealized case where a uniform free stream is assumed. The results of this study indicate that flow nonuniformities are at least partially responsible for discrepancies observed at low Reynolds number (Re/L = 1.0 $\times$ $10^6$/ft) on slender axisymmetric bodies at zero angle of attack. There is no corresponding effect at high tunnel Reynolds number (Re/L = 3.5 $\times$ $10^6$/ft). At high Reynolds number, for angles of attack that displace the nose of the vehicle more that 6-7 in. from the tunnel centerline, there is a small increase in surface pressure caused by a radial variation in Mach number.

## Nomenclature

| | | |
|---|---|---|
| $C_p$ | - | Pressure coefficient, $(P - P_\infty)/(0.5\rho Q_\infty)$ |
| e | - | Internal energy/unit volume, $ft^2/sec^2$ |
| Re | - | Reynolds number, dimensionless |
| L | - | Body length, in. |
| M | - | Mach number, dimensionless |
| P | - | Pressure, psi |
| Q | - | Total velocity, ft/sec |
| S | - | Circumferential distance, in. |
| $S_{MAX}$ | - | Circumferential distance around Half Body |
| T | - | Temperature, °R |
| U | - | X- component of velocity, ft/sec |
| V | - | Y-component of velocity, ft/sec |
| W | - | Z-component of velocity, ft/sec |
| X | - | Axial Model Coordinate, in. |
| Y,Z | - | Lateral model coordinates, in. |
| $X_T$ | - | Axial tunnel coordinates, in. |
| $Y_T$,$Z_T$ | - | Lateral tunnel coordinates, in. |
| $\alpha$ | - | Angle of attack, deg |
| $\rho$ | - | Density, $slugs/ft^3$ |
| $\theta_C$ | - | Cone half-angle, deg |

## Introduction

In several recent tests in AEDC Tunnel B at Mach 8, there have been discrepancies observed between the measured surface pressure data and computed or theoretical results. For example, Fig. 1[1] presents a comparison of measured and computed pressures on the Hypersonic Lifting Body (HLB) configuration shown in Fig. 2. The test program on this configuration was specifically designed to produce an experimental database for CFD code validation. Figure 3 taken from Ref. 2 represents a second example and shows a comparison of measured and computed pressure on two axisymmetric bodies designed to produce linear axial pressure distributions. The forebody for both of these axisymmetric bodies is a 7-deg cone.

This seemingly consistent bias for surface pressure data above expected values was considered

* The research reported herein was performed by the Arnold Engineering Development Center (AEDC), Air Force Materiel Command. Work and analysis for this research were performed by personnel of Sverdrup Technology, Inc., AEDC Group, technical services contractor for AEDC. Further reproduction is authorized to satisfy needs of the U. S. Government.

** Senior Member, AIAA.

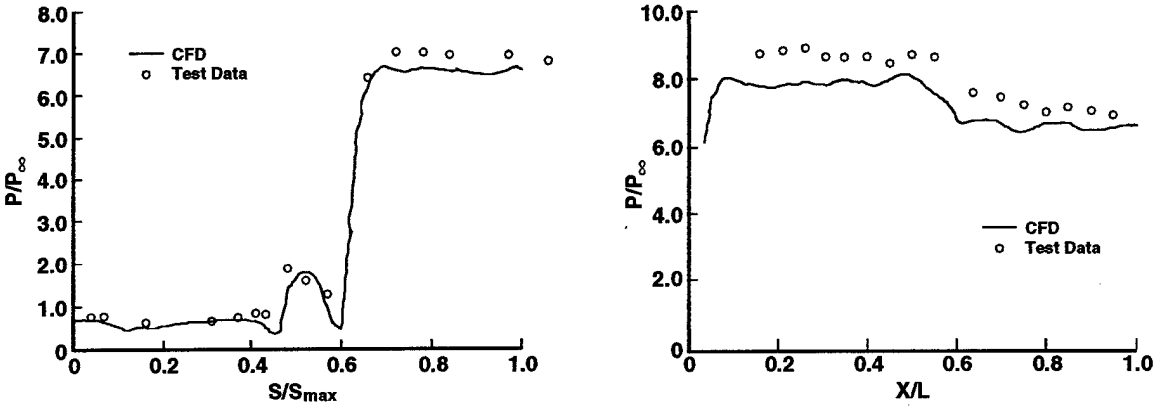


a. Circumferential pressure distribution

b. Wind side pressure distribution

Figure 1. Comparison of computed and measured pressures on hypersonic lifting body $\alpha = 10$.[1]

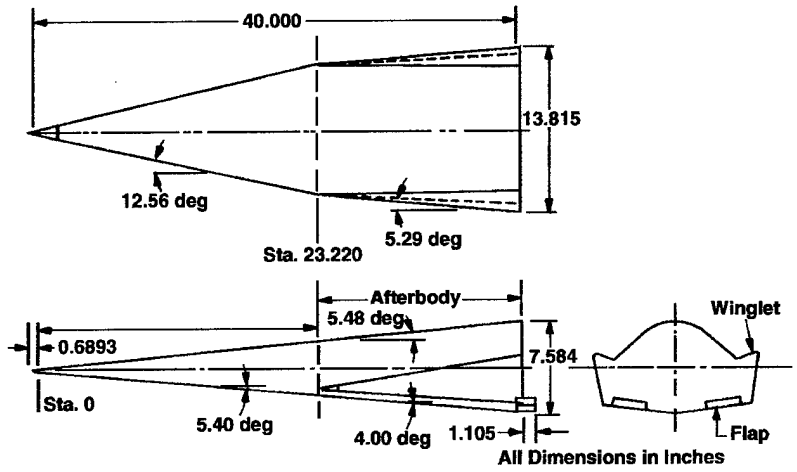


Figure 2. Hypersonic Lifting Body configuration.

sufficiently troubling to warrant investigation. This paper addresses whether, nonuniformity in the Tunnel B flow can be responsible, wholly or in part, for the observed discrepancy.

The general approach used in this study was to assess the effect of a nonuniform free-stream flow with computations. This was done by using the measured tunnel flow field as an inflow boundary condition for a CFD solution to compare with the idealized case where a uniform free stream is assumed.

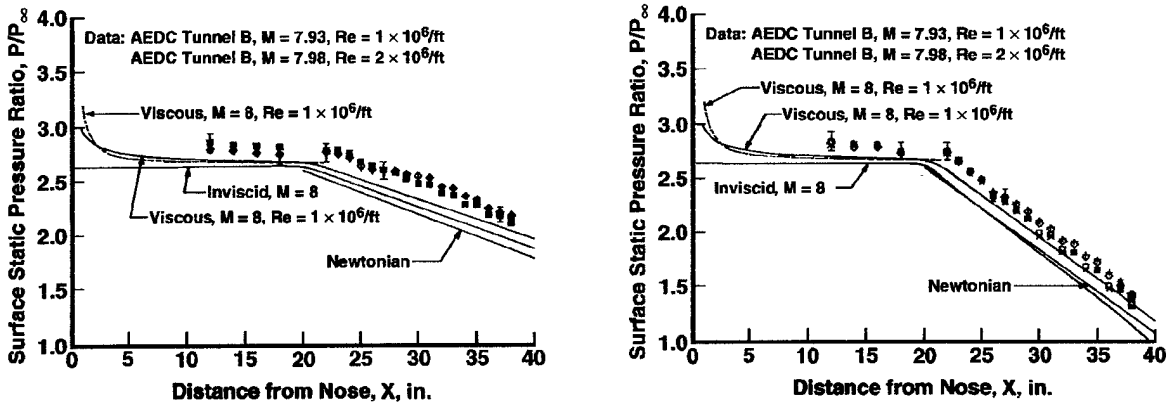


a. Surface static pressure data and theory for the small favorable-gradient body

b. Surface static pressure data and theory for the large favorable-gradient body

Figure 3. Pressure distributions on axisymmetric bodies.[2]

Two test configurations were chosen for study: a 7-deg cone at zero angle of attack based on the differences shown in Fig. 3, and the Hypersonic Lifting Body shown in Fig. 2.

## Approach

The AEDC Tunnel B is a continuous flow closed-circuit, hypersonic wind tunnel with a 50-in.-diam test section. This wind tunnel, which is described in Ref. 3, has available axisymmetric contoured nozzles to produce test section flows with nominal Mach numbers of 6 and 8. A thorough calibration of Tunnel B, documented in Ref. 4, was carried out in 1991. Pitot pressure surveys, total temperature surveys, and flow angularity measurements were obtained as a part of this effort. Survey data was taken at unit Reynolds numbers of 1.0, 2.0, and 3.5 × $10^6$. In carrying out CFD computations, initial distributions of five flow variables are required: ($\rho$, $\rho U$, $\rho V$, $\rho W$, and $\rho(e+Q^2/2)$). Pitot pressure and total temperature measurements are sufficient to determine local values of $\rho$, U, P, and T. The cone (Mach-Flow Angularity) probe provides information on the V and W velocity components. On the rake, there were 42 active pitot probes, 25 shielded total temperature probes, and 3 MFA probes. The scarcity of the cone probe data did not permit specification of the V and W velocity components. These were assumed to be zero at the inflow computational plane.

The CFD solutions for this study were generated using the STUFF code documented in Ref. 5. This flow solver was selected because it has been used extensively at AEDC for supersonic flow computations and is known to produce reliable results for a variety of configurations and test conditions. It was also relatively easy to adapt the code to accept the measured free-stream conditions. Although STUFF has a nonequilibrium capability, all of the computations in this study assumed perfect air.

In this paper, it is necessary to refer to both tunnel coordinates and model coordinates. Wind tunnel coordinates designated by a subscript T are defined in Fig. 4a, which represents a sketch of the test section of Tunnel B. Model coordinate definitions and their relationship to tunnel coordinates are presented in Fig. 4b.

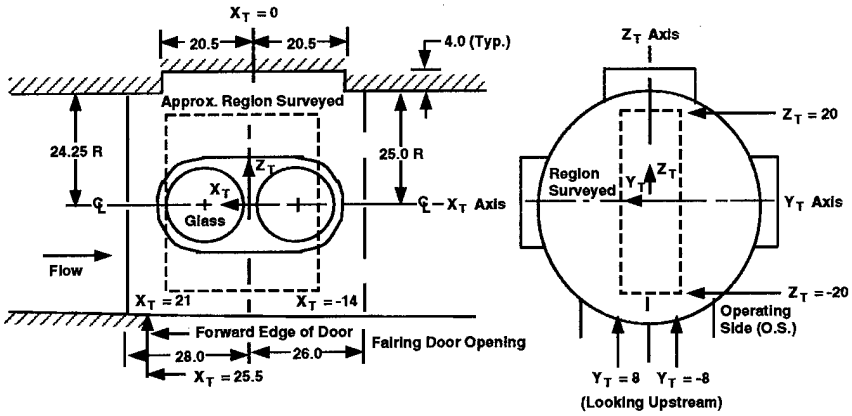


a. Wind tunnel coordinates

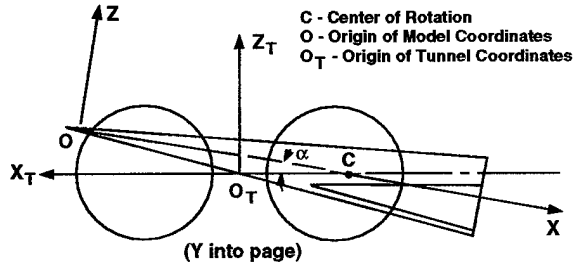


b. Model coordinates

Figure 4. Tunnel and model coordinate systems.

The primary calibration data used in this paper is derived from the rake. The 42 pitot probes covered a range from $Z_T$ = -20 to $Z_T$ = +19.8 in. and the 25 temperature probes spanned $-16.2 \le Z_T \le 15.8$. The rake could be traversed in the axial ($X_T$) direction or the lateral ($Y_T$) direction. Figures 5 and 6 show examples of the pitot pressure and total temperature rake data from a lateral survey and

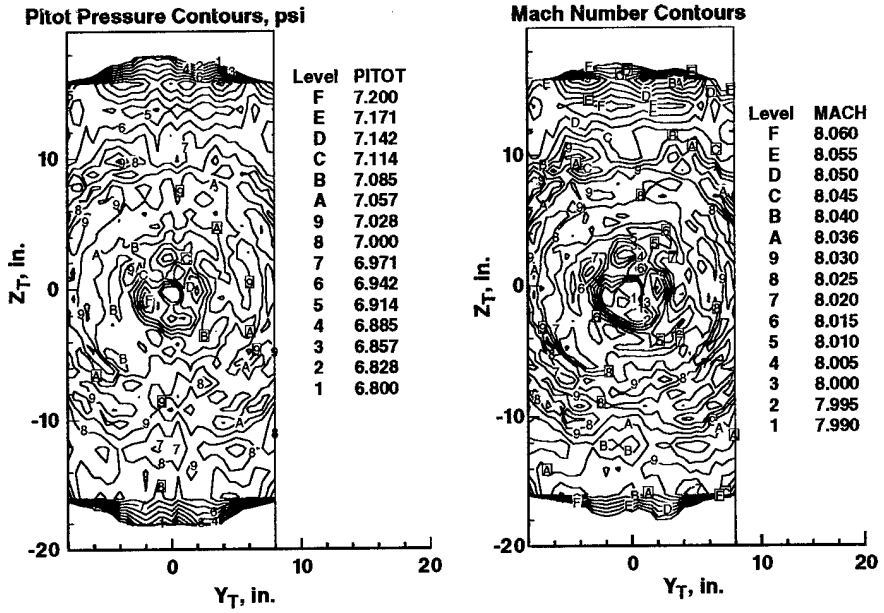


a. Pitot pressure

b. Local Mach number

Figure 5. Rake pitot measurements, $X_T$ = 16 in.

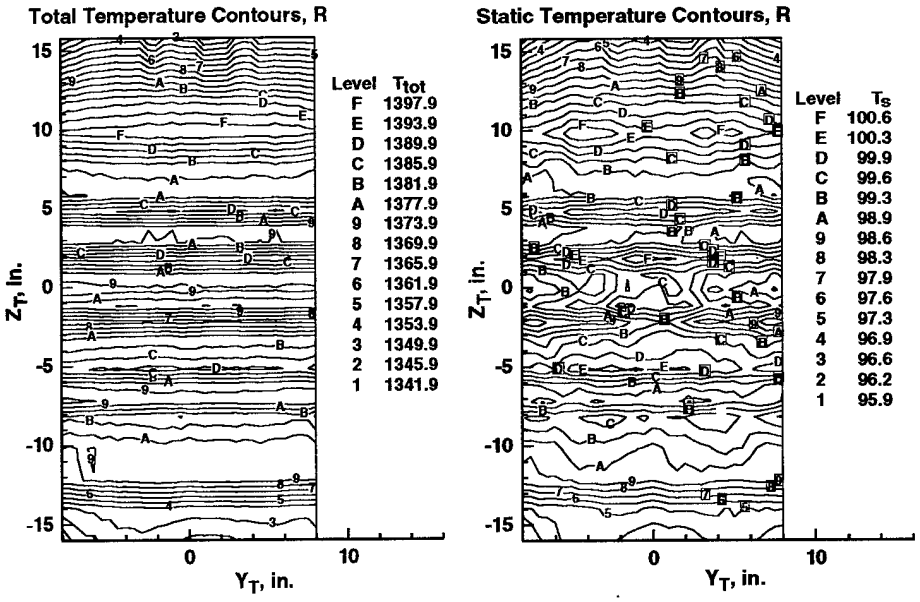


a. Local total temperature

b. Static temperature

Figure 6. Rake temperature measurements, $X_T$ = 16 in.

the Mach number and static temperature contours extracted from that data. The fact that the total temperature contours are parallel to the direction of rake travel indicates that these measurement are influenced by probe-to-probe bias. Numerical experiments have shown that model surface pressures are only slightly affected by the total temperature variations, and the computed pressure results reported herein would not be measurably changed if the local total temperature values presented in Fig. 6 were replaced by a constant, $T_0$ = 1350°R, the reservoir temperature.

Unfortunately, lateral surveys such as shown in Figs 5 and 6 were performed at only a few stations. The farthest upstream station available is that shown, $X_T$ = 16 in. An axial survey at $Y_T$ = 0 extended from $X_T$ = 21 to $X_T$ = -14 in. A difficulty encountered in carrying out the approach was that for the long, slender configurations under study, the nose of the model extended beyond the range of survey data. Specifying initial conditions for the computations was handled differently for the two different configurations. For the 7-deg cone, the farthest upstream data station, $X_T$ = 21, from the axial survey was used for the initial conditions. Moreover, since lateral date was not available and the cone was mounted on the tunnel centerline, the flow field was assumed to be axially symmetric. For the nonsymmetric Hypersonic Lifting Body, the lateral survey data at $X_T$ = 16 was assumed to apply at the model nose at about $X_T$ = 21.

For the 7-deg cone, computations were carried out primarily for a unit Reynolds number of $1.0 \times 10^6$ since much of the data of Ref. 2 was acquired at that value. At this Reynolds number, viscous computations can be performed without the complicating factors of boundary layer transition and turbulence modeling. For the Hypersonic Lifting Body most of the data were acquired at Re/L = $3.5 \times 10^6$/ft with boundary layer trips installed. The majority of the computations carried out for this configuration were performed assuming an inviscid fluid but with initial conditions corresponding to a unit Reynolds number of $3.5 \times 10^6$/ft.

Figure 7 shows measured pitot profiles at $X_T$ = 21.25 for the lowest Reynolds number and the Mach number distributions calculated from the pitot pressures and the measured reservoir pressure. The drop in pitot pressure for $|Z_T| > 15$ is clearly

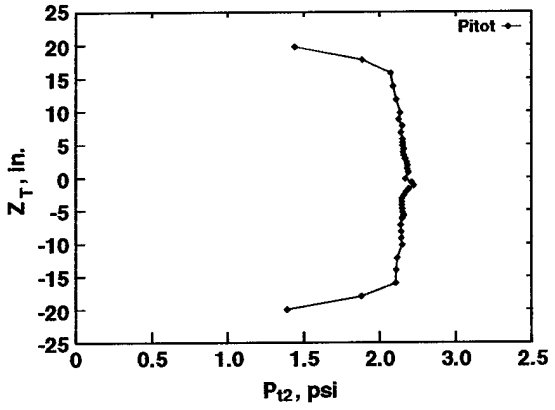


a. Pitot pressure

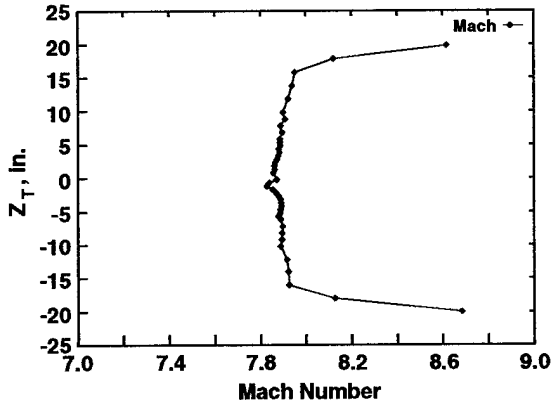


b. Mach number distribution

Figure 7. Pitot pressure and Mach number distribution, XT = 21.245 in., Re = $1.0 \times 10^6$ ft.

due to the tunnel wall boundary layer. The data reduction procedure, which assumes inviscid flow, produces an incorrect increase in Mach number as the wall is approached. In the present work, no attempt was made to account for the wall boundary layer in the computations - only the inviscid core flow was treated. The test section area-weighted Mach number for this flow condition was determined in the calibration to be 7.934.

## Results and Discussion

### Empty Tunnel

Figure 8 shows some of the initial profiles that were used in the computations for the 7-deg cone. The flow was assumed to be axisymmetric and the initial values were interpolated from the measurements on the initial ray of the computational grid. The computational grid extended from the tunnel axis to the wall. However, as discussed earlier, no attempt was made to model the tunnel wall boundary layer. Thus the data at what was judged to be the last point outside the boundary layer was repeated at the wall for interpolation purposes.

The first computation was performed for an empty tunnel to compare with rake calibration data farther downstream in the test section. The results of these computations are shown in Fig. 9. The agreement between the computations and the data is quite good with the exception of the last data point shown. The pressure and density increase at this point is the result of a compression wave that originates far upstream in the nozzle and represents the edge of the test rhombus. The good agreement shown in Fig. 9 lends credibility to the computational technique and indicates that no unwarranted assumptions have been made.

### 7-deg Sharp Cone

The next set of computations that will be discussed are for a 7-deg sharp cone positioned on the tunnel axis with the apex located at $X_T$ = 21.25 in. The computational grid for this configuration is shown in Fig. 10 and was used for calculations assuming both an inviscid and viscous fluid. The clustering of coordinate lines at the wall is necessary with a viscous fluid to resolve the wall bound-

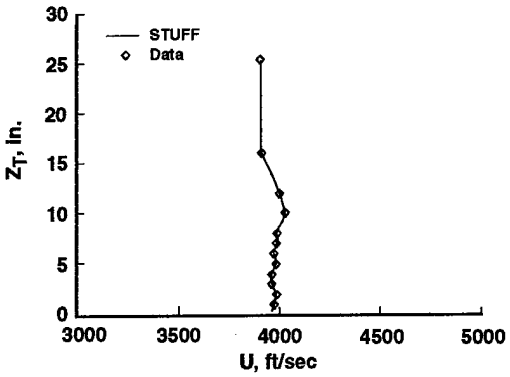


a. Velocity distribution

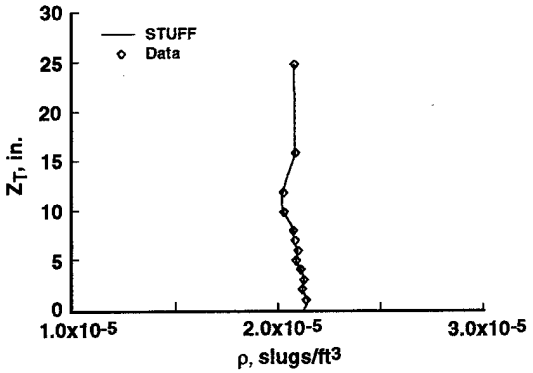


b. Density distribution

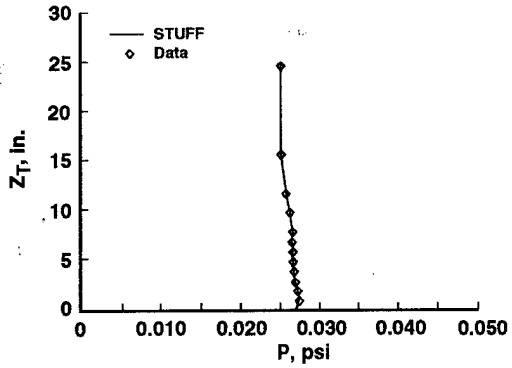


c. Pressure distribution

Figure 8. Initial computational profiles, XT = 21.25.

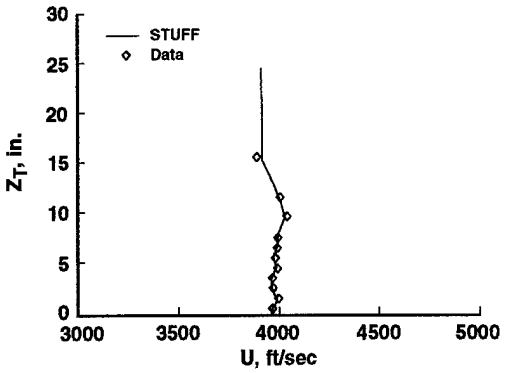


a. Velocity distribution

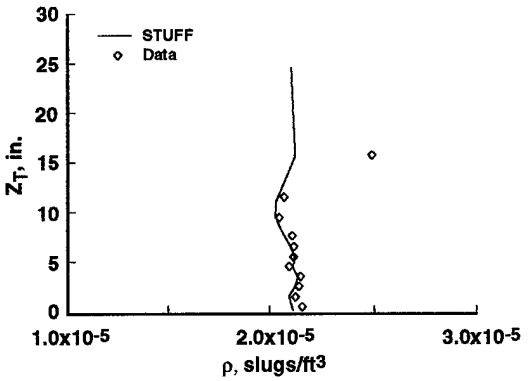


b. Density distribution

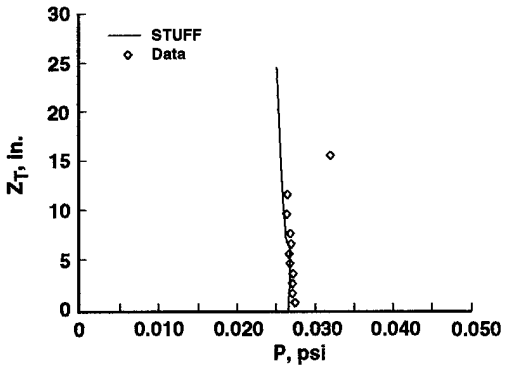


c. Pressure distribution

Figure 9. Comparison of computations with data for empty tunnel, $X_T$ = -14.

ary layer. For a shock capturing flow solver, as being used in the present study, on a sharp body, radial grid clustering is also helpful in capturing the bow shock near the apex. To illustrate, Fig. 11 shows pressure contours from a computation for an inviscid fluid and a uniform freestream.

The effect of the nonuniform free stream on the cone pressure for a Reynolds number of $1.0 \times 10^6$/ ft is shown in Fig. 12. Figure 12a shows a comparison of inviscid computations with the measured initial profiles with the idealized case of a uniform free stream. The theoretical cone pressure[6] or a Mach

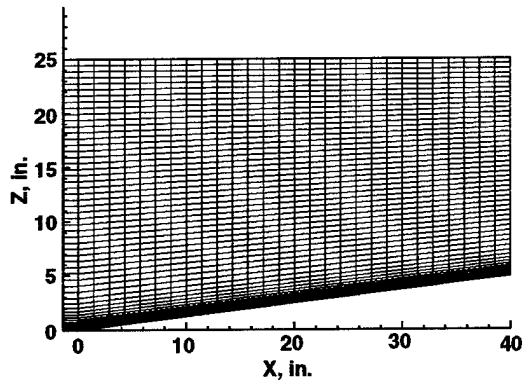


Figure 10. Computational grid $\theta_c = 7$ deg.

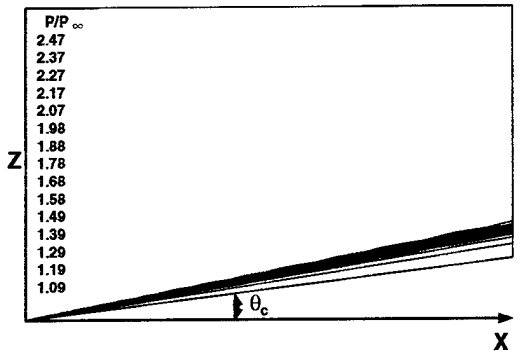


Figure 11. Pressure contours inviscid flow, uniform free stream.

number of 7.934 is also shown in the plot. There is a definite increase in cone surface pressure caused by the non-uniform free stream. Figure 12b shows results from a similar computation assuming a laminar boundary layer on the cone. The difference between the pressure distributions for the

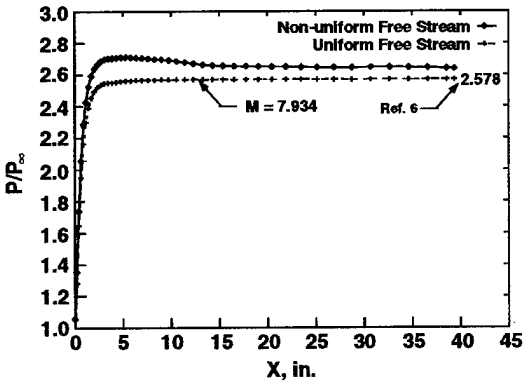


a. Inviscid flow

Figure 12. Effect of non-uniform free-stream flow on cone pressure.

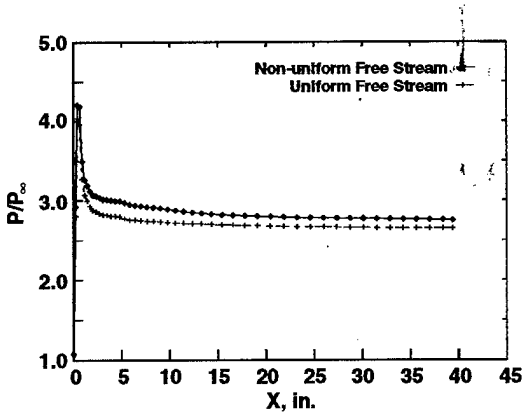


b. Laminar flow

Figure 12. Concluded.

uniform and nonuniform free stream is approximately the same for the viscous and inviscid calculations.

Figure 13 shows a comparison of the nonuniform free-stream CFD results for a laminar boundary layer with a compilation of data for a 7-deg cone. The bulk of the data shown is forecone data previously presented in Fig. 3 Some additional data at higher Reynolds number that is thought to be laminar has been included. The computational results represent the data as well as can be expected.

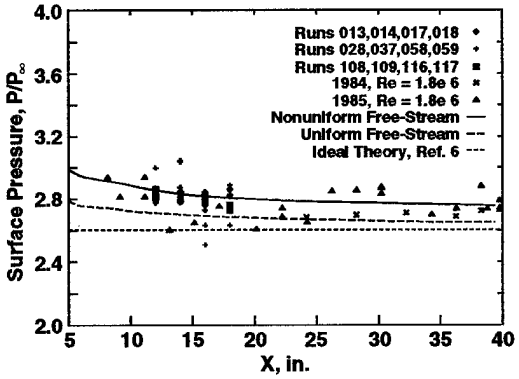


Figure 13. Computational results with nonuniform free-stream compared to 7-deg cone data.

The effect of a nonuniform free-stream on the inviscid pressure distribution at a unit Reynolds number of $3.5 \times 10^6$/ft is shown in Fig. 14. Although the computations assume an inviscid fluid, the initial flow distribution depends on tunnel Reynolds

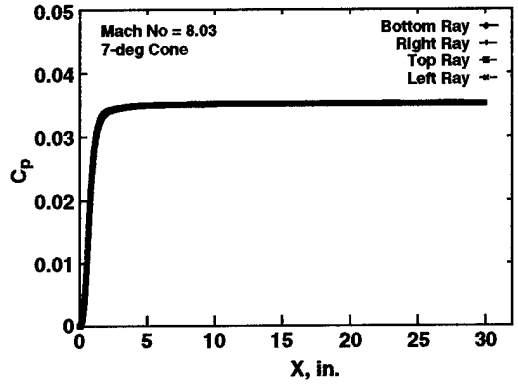


a. Uniform initial profiles

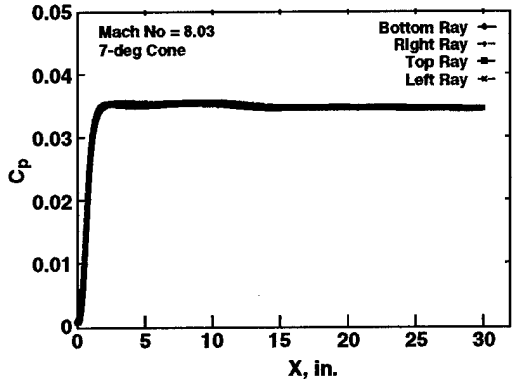


b. Measured initial profiles

Figure 14. Effect of initial profiles on cone pressure at Re = $3.5 \times 10^6$ ft.

number. This computation uses initial data derived from Figs. 5 and 6 and takes into account the three-dimensional character of the flow. The pressure distribution for the measured initial profiles is virtually identical to that for a uniform free stream. Thus the effect of a nonuniform free stream appears to be much less at the high Reynolds number than at low Reynolds number. Presumably, the smaller displacement thickness on the nozzle wall at high Reynolds number results in somewhat better flow quality.

### Hypersonic Lifting Body

Results were computed for the HLB configuration for the range of positive angles of attack covered by the experimental program. Three cross-sectional planes from an example grid used for the computations at an angle of attack of 10 degs are shown in Fig. 15. The outer boundary of the grid is a cylinder of radius 15 in. that is parallel to the tunnel axis. A 30-in.-diam circle includes the region covered by the rake survey, except for the areas where the tunnel wall boundary layer intrudes.

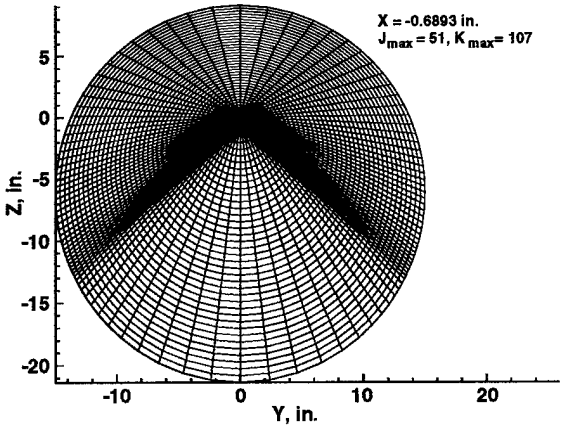


a. Cross-sectional grid - X = 0.6893 in.

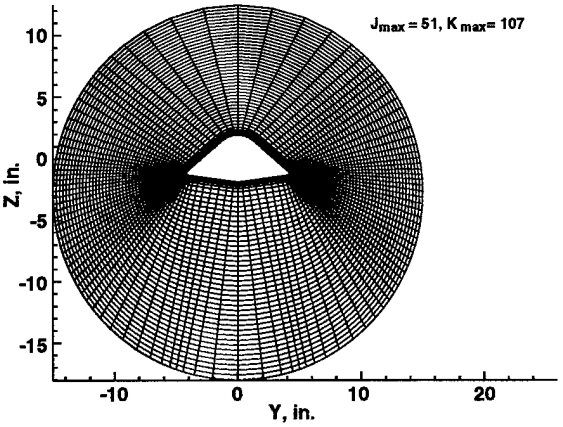


b. Cross-sectional grid - X = 18.09 in.

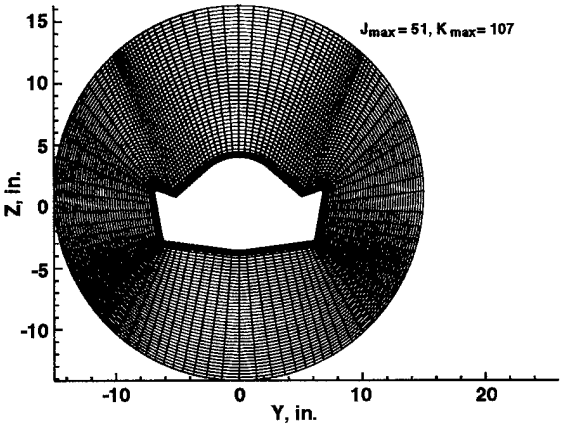


c. Cross-sectional grid - X = 40.0 in.

Figure 15. Example cross-sectional grids for HLB at $\alpha$ = 10 deg.

Constructing a grid for the model in the tunnel required knowledge of the location of the center of rotation (see Fig. 4) in model coordinates and tunnel coordinates. The test project engineer provided these values ($X_C = 34$, $Y_C = 0$, $Z_C = 0$, $X_{TC} = -18$, $Y_{TC} = 0$, $Z_{TC} = 0$).

Figure 16 shows inviscid computational results for both a uniform and nonuniform free stream compared with measured pressure data for 10-deg angle of attack. There is very little difference between the two computations, both being about 10 percent below the data on the wind side. Similar computational results for a 15-deg angle of attack are presented in Fig. 17. For this case there is a noticeable increase in wind-side pressure due to the nonuniform free stream. This increase is

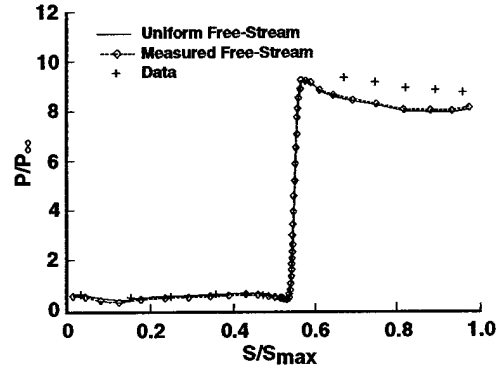


a. X/L = 0.55

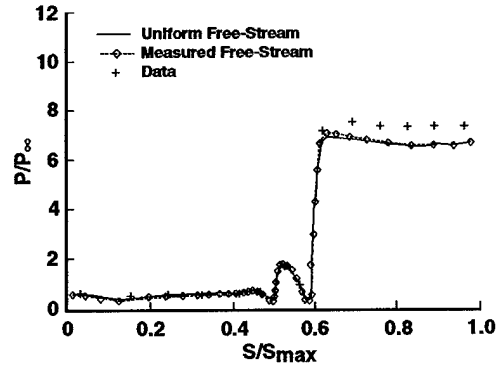


b. X/L = 0.70

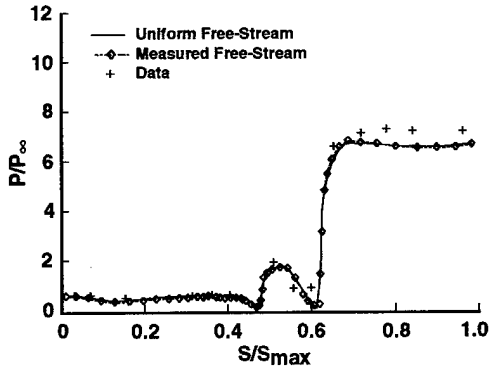


c. X/L = 0.80

Figure 16. Circumferential pressure distributions, inviscid computations, $\alpha = 10$ deg.

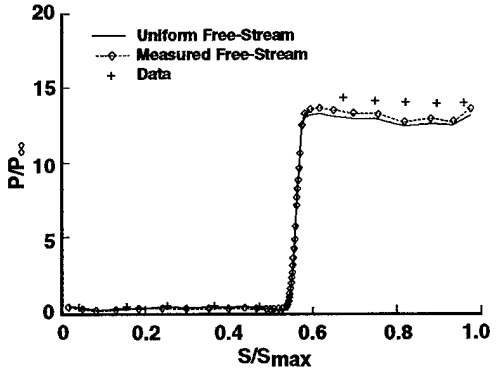


a. X/L = 0.55

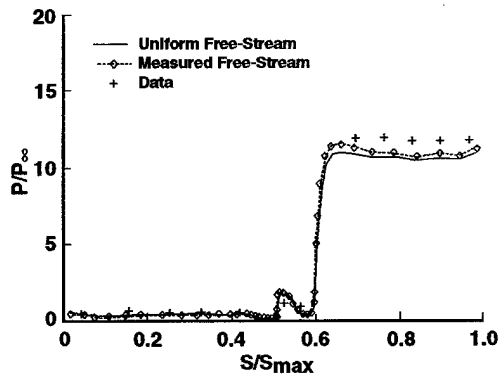


b. X/L = 0.70

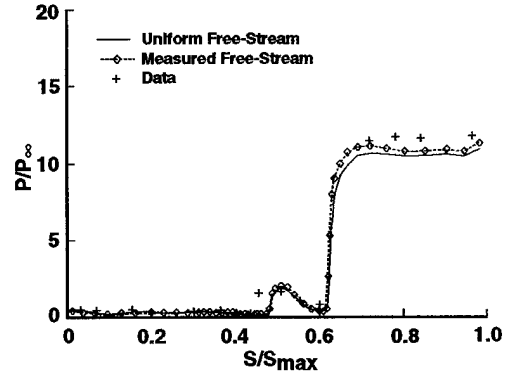


c. X/L = 0.80

Figure 17. Circumferential pressure distributions, inviscid computations, $\alpha = 15$ deg.

thought to be due to the fact that the nose and forebody of the vehicle at this angle of attack were positioned far enough from the tunnel centerline to encounter a slightly higher Mach number flow (cf. Fig. 5). The computed values on the wind side are still significantly below the data.

Unfortunately, the computations could not be completed over the entire vehicle for 20-deg angle of attack due to negative densities encountered on the lee surface. Comparisons of inviscid computations with pressure data at X/L = 0.25 and X/L = 0.55 shown in Fig. 18 reveal a noticeable effect of the wind side due to the nonuniform free stream. The computational results for a nonuniform free stream are definitely approaching the data as angle of attack increases. This is almost certainly due to the radial distributions of Mach number shown in Fig. 5.

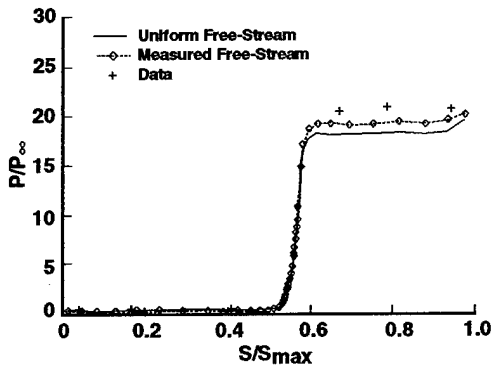


a. X/L = 0.25

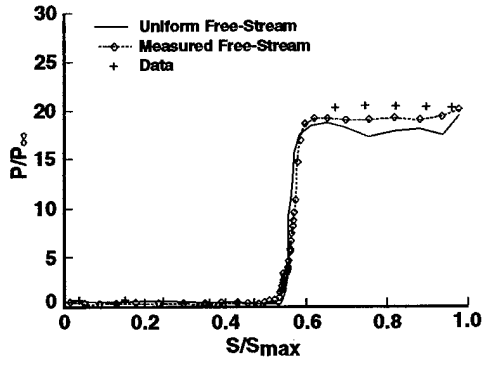


b. X/L = 0.55

Figure 18. Circumferential pressure distributions, inviscid computations, $\alpha$ = 20 deg.

## Summary and Conclusion

The results of this study indicate that flow nonuniformities are at least partially responsible for discrepancies observed between measured and computed surface pressures at low Reynolds number (Re/L = 1.0 × $10^6$/ft) on slender axisymmetric bodies at zero angle of attack. There is no corresponding effect at high tunnel Reynolds number (Re/L = 3.5 × $10^6$/ft). Presumably, the flow quality is better at high Reynolds number due to a thinner tunnel wall boundary layer. Even a high Reynolds number, however, for angles of attack that displace the nose of the vehicle more that 6-7 in. from the tunnel centerline, there is a small increase in surface pressure caused by a radial variation in Mach number. Presumably, yaw or lateral displacements would cause a similar effect.

The effect due to radial Mach number variations is not sufficient to explain fully the pressure discrepancies HLB observed, although the trend with increasing angle of attack is in the right direction. Other possible sources of the discrepancy, although unlikely, are (1) model/sting deflections, (2) flow angularity (neglected in this study), (3) differences between the computational model and the tunnel model geometry, (4) a consistent bias in the pressure measurements, and (5) errors in the computations. One is reluctant to focus on computational errors because other investigators using different codes have found similar results.

## References

1. Le, A. T., Shivananda, T. P., Holtz, T., and Marx, R. S. "CFD Predictions of Flowfields About a Hypersonic Lifting Body." AIAA-93-3692, August 1993.

2. Shope, F. L. and Spinetti, R. L. "Aerodynamic Design of a Hypersonic Body with a Constant Favorable Pressure Gradient." AIAA-93-3444, August 1993.

3. Anderson, A and Matthews, R. K. "Aerodynamic and Aerothermal Facilities I, Hypersonic Wind Tunnels." *Methodology of Hypersonic Testing*, VKI/AEDC Special Course, February 1993.

4. Strike, W. T., Coulter, S. M., and Mills, M. L. "A 1991 Calibrations of the AEDC Hypersonic Wind Tunnels (Nozzle Mach Numbers 6, 8 and 10)." AIAA-92-5092, November 1992.

5. Molvik, G. A. and Merkle, C. L. "A Set of Strongly Coupled, Upwind Algorithms for Computing Flows in Chemical Nonequilibrium." AIAA-89-0199, January 1989.

6. Ames Research Staff, "Equations, Tables, and Charts for Compressible Flow." NACA Report 1135, 1953.

# REPORT DOCUMENTATION PAGE

*Form Approved*
*OMB No. 0704-0188*



| 1. AGENCY USE ONLY *(Leave blank)* | 2. REPORT DATE | 3. REPORT TYPE AND DATES COVERED |
|---|---|---|
| | January 1997 | Technical Society Paper, Oct 1995, Sept 1996 |

**4. TITLE AND SUBTITLE**
Investigation of Differences Between Measured and Predicted Pressures in AEDC/VKF Hypersonic Tunnel B
AIAA Paper No. 97-0566

**5. FUNDING NUMBERS**

**6. AUTHOR(S)**
James R. Maus

**7. PERFORMING ORGANIZATION NAME(S) AND ADDRESS(ES)**
Sverdrup Technology, Inc., AEDC Group
Arnold Engineering Development Center
Arnold Air Force Base, TN 37389

**8. PERFORMING ORGANIZATION REPORT NUMBER**

**9. SPONSORING/MONITORING AGENCY NAME(S) AND ADDRESS(ES)**
USAF/AFMC/AEDC/DOS
Arnold AFB, TN 37389

**10. SPONSORING/MONITORING AGENCY REPORT NUMBER**

**11. SUPPLEMENTARY NOTES**
Presented at 35th Aerospace Sciences Meeting and Exhibit in Reno, NV.

**12a. DISTRIBUTION AVAILABILITY STATEMENT**
Approved for public release; distribution unlimited.

**12b. DISTRIBUTION CODE**
A

**13. ABSTRACT** *(Maximum 200 words)*

A study has been carried out to assess the effect of flow nonuniformities in AEDC Tunnel B on surface pressures of slender bodies. The approach taken was to use flow profiles measured in a recent calibration program as inflow boundary conditions for a CFD solution to compare with the idealized case where a uniform free stream is assumed. The results of this study indicate that flow nonuniformities are at least partially responsible for discrepancies observed at low Reynolds number (Re/L = 1.0 x 10 6 /ft) on slender axisymmetric bodies at zero angle of attack. There is no corresponding effect at high tunnel Reynolds number (Re/L = 3.5 x 10 6 /ft). At high Reynolds number, for angles of attack that displace the nose of the vehicle more that 6-7 in. from the tunnel centerline, there is a small increase in surface pressure caused by a radial variation in Mach number.

| 14. SUBJECT TERMS | 15. NUMBER OF PAGES |
|---|---|
| CFD, flow nonuniformities, surface pressure | 12 |
| | 16. PRICE CODE |

| 17. SECURITY CLASSIFICATION OF REPORT | 18. SECURITY CLASSIFICATION OF THIS PAGE | 19. SECURITY CLASSIFICATION OF ABSTRACT | 20. LIMITATION OF ABSTRACT |
|---|---|---|---|
| Unclassified | Unclassified | Unclassified | UL |